

weaker,^{10,23} and the molecules consequently are less puckered, i.e., approaching the structure of the $S_4N_4^{2+}$ dication.²⁴ In such a conformation the cross-ring interactions between 1,5 sulfurs and their ligands will be less restrictive, and equilibration of the ligand orientations can occur.

Conclusion

The broad range of chemical shifts exhibited by the compounds examined in this preliminary study illustrate the sensitivity of the ^{15}N nucleus to changes in molecular and electronic environment. Although the interpretation of these shifts is not straightforward, the information presented here provides an empirical basis for the identification of both new and known

sulfur-nitrogen species. The complex solution chemistry of sulfur-nitrogen derivatives can now be routinely monitored in ^{15}N NMR spectroscopy, and the study of the fluxional behavior of sulfur-nitrogen rings and cages (e.g., $S_4N_5^{\pm}$ and $S_3N_6^{2\pm}$) can be pursued. We are currently investigating these possibilities.

Acknowledgment. We thank the Natural Sciences and Engineering Research Council of Canada, the University of Calgary, and NATO (Research Grant No. 1744) for financial support. The assistance of Dr. R. Yamdagni in obtaining the NMR spectra and helpful discussions with Dr. W. G. Laidlaw are gratefully acknowledged. We also thank Dr. J. Mason for her comments on the manuscript.

Registry No. $Me_3SiNSNSiMe_3$, 18156-25-7; S_4N_4 , 28950-34-7; S_4N_2 , 32607-15-1; $S_4N_3^+$, 29631-23-0; $Ph_3P=NS_3N_3$, 33082-06-3; $Ph_3As=NS_3N_3$, 63212-45-3; $Ph_3P=NSNS$, 73845-61-1; 1,5-($Ph_3P=N$) $_2S_4N_4$, 72144-79-7; $Cl_2S_4N_4$, 71699-97-3; $Cl_3S_3N_3$, 5964-00-1; S_4N_3Cl , 67954-28-3; $S_4N_5^-$, 58858-09-6; $S_3N_3^-$, 65107-36-0; S_4N^- , 51330-98-4; S_4N_3Cl , 12015-30-4; ^{15}N , 14390-96-6.

- (23) Bartetzko, R.; Gleiter, R. *Chem. Ber.* **1980**, *113*, 1138.
 (24) Gillespie, R. J.; Slim, D. R.; Tyrer, J. D. *J. Chem. Soc., Chem Commun.* **1977**, 253.
 (25) Recent low-temperature studies on $S_4N_4Cl_2$ indicate that the two chlorines are nonequivalent below ca. 0 °C. Chivers, T.; Oakley, R. T., unpublished results.

Contribution from the Research Institute for Materials, University of Nijmegen, Nijmegen, The Netherlands, and the Department of Chemistry, State University of Leiden, Leiden, The Netherlands

Ferromagnetic Exchange Coupling in Polynuclear Copper(I)-Copper(II) Complexes with Penicillamine and Related Ligands

HERMAN VAN KEMPEN,^{1a} JOS A. A. J. PERENBOOM,^{*1a} and PAUL J. M. W. L. BIRKER^{1b}

Received May 8, 1980

Crystalline derivatives of mixed-valence Cu(I)-Cu(II) cluster complexes of composition $[Cu^II_6Cu^I_8L_{12}Cl]^{5-}$, where L is deprotonated α -mercaptoisobutyric acid or D-penicillamine, were obtained with $Co(NH_3)_6^{3+}$ as counterions. The magnetic moments of these complexes have been measured in the temperature range from 2.5 to 300 K and in magnetic fields up to 2.0 T. A ferromagnetic interaction was observed which is interpreted as due to *intracluster-exchange* interactions between the spins of the six paramagnetic Cu(II) atoms which are located at the apices of a slightly deformed octahedron with edges of ~ 0.67 nm. A theoretical model is discussed which describes the interaction of spins in a locally isolated, symmetrical arrangement. A model of isotropic Heisenberg nearest-neighbor-exchange interactions for an octahedral arrangement of spins gives a good fit with the experimental data for an exchange constant J/k_B on the order of 7 K.

Introduction

Mixed-valence copper complexes of composition $[Cu^II_6Cu^I_8L_{12}Cl]^{2-}$ have been synthesized with three thiolate ligands (L), viz., D-penicillamine^{2,3} [$H_2Pen = HSC-(CH_3)_2CH(NH_3^+)COO^-$; $z = 5^-$], β,β -dimethylcysteamine^{4,5} [$HDMC = HSC(CH_3)_2CH_2NH_2$; $z = 7^+$], and α -mercaptoisobutyric acid⁶ [$H_2MIBA = HSC(CH_3)_2COOH$; $z = 5^-$]. These complexes have been characterized by X-ray diffraction, and their geometries have been described.²⁻⁶ They have a number of structural features in common (Figure 1). A single chlorine atom lies at the center of a cube of eight Cu(I) atoms. This Cu^I_8 cube is inscribed into an icosahedron of 12 sulfur atoms, so that each Cu(I) atom lies at the center of a triangular face of this S_{12} icosahedron. Above each of the six faces of the Cu^I_8 cube lies a Cu(II) atom. The Cu(II) atoms lie also above a S-S edge of the sulfur icosahedron. Each sulfur atom

forms a bridge between two Cu(I) atoms and one Cu(II) atom. The bidentate ligands chelate the Cu(II) atoms resulting in cis planar four-coordination ($Cu^IIN_2S_2$ for H_2Pen and $HDMC$; $Cu^IIS_2O_2$ for H_2MIBA). The methyl substituents are essential as they protect the Cu(I) sites sterically.³ The six Cu(II) atoms occupy the vertices of a slightly deformed octahedron with edges of approximately 0.67 nm.²⁻⁶

These compounds are unique examples of systems in which a large number (six) of relatively isolated paramagnetic centers are symmetrically arranged in a single molecule.

The ESR spectra of the H_2Pen ³ and $HDMC$ ⁵ complexes are poorly resolved. Most likely this is due to intramolecular interactions between the paramagnetic Cu(II) atoms. We will discuss a very general approach to the description of the magnetic *intracluster-exchange* interactions in polynuclear paramagnetic complexes. The calculations are carried out in detail for a regular octahedral arrangement of spins. The analysis of the data on the temperature dependence of the magnetic susceptibility for the H_2Pen and for the H_2MIBA complexes based on this model reveals the existence of a ferromagnetic interaction. The magnetic field dependence of the magnetization data at our lowest temperatures indicates that the lowest level is characterized by a spin quantum number $S = 3$.

Recently a ferromagnetic exchange interaction was reported for the corresponding $HDMC$ complex.⁵ In the model used

- (1) (a) University of Nijmegen. (b) State University of Leiden.
 (2) Birker, P. J. M. W. L.; Freeman, H. C. *J. Chem. Soc., Chem. Commun.* **1976**, 312.
 (3) Birker, P. J. M. W. L.; Freeman, H. C. *J. Am. Chem. Soc.* **1977**, *99*, 6890.
 (4) Schugar, H. J.; Ou, C.; Thich, J. A.; Potenza, J. A.; Lalancette, R. A.; Furey, W., Jr. *J. Am. Chem. Soc.* **1977**, *99*, 6890.
 (5) Schugar, H. J.; Ou, C. C.; Thich, J. A.; Potenza, J. A.; Felthouse, T. R.; Haddad, M. S.; Hendrickson, D. N.; Furey, W., Jr.; Lalancette, R. A. *Inorg. Chem.* **1980**, *19*, 543.
 (6) Birker, P. J. M. W. L. *Inorg. Chem.* **1979**, *18*, 3502.

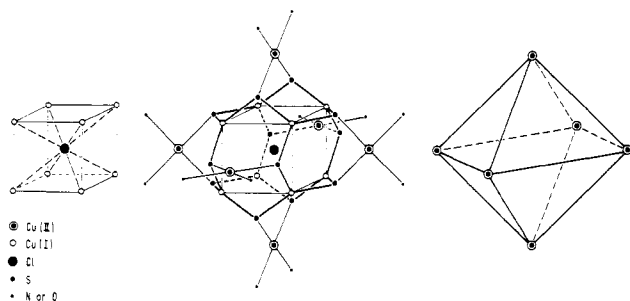


Figure 1. Structure of the mixed-valence clusters. Only the $[\text{Cu}^{\text{II}}_6\text{Cu}^{\text{I}}_8\text{S}_{12}(\text{N/O})_{12}\text{Cl}]$ part of the complex is shown. The Cu^{I}_8 cube with the central Cl atom and the Cu^{II}_6 octahedron are shown separately on the same scale. Drawings of the complete complex ions including all ligands can be found in ref 2-6.

to describe the temperature dependence of the magnetic susceptibility of this complex the magnetic field dependence was not taken into account. Although the measurements were carried out at 1.2 T and not below 4.2 K, saturation effects are significant. In the present work measurements have been done over a range of magnetic field strengths (up to 2.0 T) and temperatures (down to 2.5 K). Both the temperature and field dependence of the magnetization of the copper compounds with H_2Pen and H_2MIBA as ligands are correctly described by our model, although there is some discrepancy left at the high-temperature side.

Experimental Section

Materials. The crude sodium salts $\text{Na}_5[\text{Cu}_{14}(\text{Pen})_{12}\text{Cl}] \cdot x\text{H}_2\text{O}$ and $\text{Na}_5[\text{Cu}_{14}(\text{MIBA})_{12}\text{Cl}] \cdot y\text{H}_2\text{O}$ were prepared as described earlier.^{2,6} All other chemicals and solvents were of reagent grade quality.

Crystallization of $[\text{Co}(\text{NH}_3)_6]_5[\text{Cu}_{14}(\text{Pen})_{12}\text{Cl}]_3 \cdot 185\text{H}_2\text{O}$. $\text{Na}_5[\text{Cu}_{14}(\text{Pen})_{12}\text{Cl}] \cdot x\text{H}_2\text{O}$ (60 mg) was dissolved in 6 mL of water in a test tube. Pure water (8 mL) was introduced above this solution with a Pasteur pipette. A solution of $\text{Co}(\text{NH}_3)_6\text{Cl}_3$ (20 mg in 6 mL of water) was carefully added to the upper layer. The crystallization was complete after 5 days. The purple-black needles were filtered off, washed with water, and dried in air. Anal. Calcd for $[\text{Co}(\text{NH}_3)_6]_5[\text{Cu}_{14}(\text{SC}_2\text{H}_9\text{NO}_2)_{12}\text{Cl}]_3 \cdot 185\text{H}_2\text{O}$: Co, 2.41; Cu, 21.85; S, 9.45; N, 7.57; C, 17.70; H, 5.58. Found: Co, 2.33; Cu, 21.55; S, 9.38; N, 7.48; C, 18.20; H, 5.05.

Crystallization of $[\text{Co}(\text{NH}_3)_6]_5[\text{Cu}_{14}(\text{MIBA})_{12}\text{Cl}]_3 \cdot 64\text{H}_2\text{O}$. $\text{Na}_5[\text{Cu}_{14}(\text{MIBA})_{12}\text{Cl}] \cdot y\text{H}_2\text{O}$ (100 mg) was dissolved in 4 mL of water in a test tube. Pure water (10 mL) was layered on top of this solution. A solution of $\text{Co}(\text{NH}_3)_6\text{Cl}_3$ (20 mg in 1 mL of water) was added to the top layer. After 24 h the first crystals had formed, and again 1 mL of the $\text{Co}(\text{NH}_3)_6\text{Cl}_3$ solution was added. After another 24 h the crystallization was complete. The brown-black needles were filtered off, washed with water, and dried in air. Anal. Calcd for $[\text{Co}(\text{NH}_3)_6]_5[\text{Cu}_{14}(\text{SC}_4\text{H}_6\text{O}_2)_{12}\text{Cl}]_3 \cdot 64\text{H}_2\text{O}$: Co, 3.28; Cu, 29.70; S, 12.84; C, 19.24; H, 4.87. Found: Co, 3.11; Cu, 29.53; S, 13.33; C, 19.45; H, 3.96.

Magnetization Measurements. We have determined the magnetic moment of the samples using a very sensitive magnetometer designed in our laboratory¹⁸ and employing a low-frequency sample position modulation (2 s^{-1}).⁷ In this experimental setup the magnetic field is generated by a superconductive solenoid. Two oppositely wound superconducting pickup coils⁸ are rigidly attached to the magnet and are positioned coaxially with the magnetic field. A continuous-flow cryostat is inserted through the pickup coils and allows regulation of sample temperature between 2.5 and 300 K. The pickup coils are part of a low-inductance superconducting circuit, the flux transformer. Such a coil geometry was used that the current generated in the fluxtransformer is linearly dependent on the position of the sample over a range of several millimeters. The current in the fluxtransformer is measured with a flux gated galvanometer of similar design as

reported by Poerschke and Wollenberger.^{7,9} The relevant low-frequency modulation at the output of the galvanometer is detected with common lock-in techniques. Inherent to the measurement technique are large contributions due to the uncompensated static flux of the applied magnetic field and of the induced magnetization of the construction materials in the vicinity of the pickup coils. The static offset of the galvanometer is kept within reasonable limits by a feedback scheme which couples the static output of the galvanometer back and by occasional heating of part of the flux transformer above the critical temperature to make the large static contributions to the current vanish. The output voltage of the instrument is proportional to the magnetic moment of the sample up to a moment of $0.5 \times 10^{-3} \text{ J/T}$ (MKSA units are used throughout this article; conversion factors to cgs units are given in ref 11). Typically samples of 50 mg can be accommodated in our sample holders. The instrument was calibrated against the saturation magnetization of a small nickel sample. The accuracy of the calibration is 1%. The noise corresponds with $\Delta m = 3 \times 10^{-9} \text{ J/T}$ ($3 \times 10^{-6} \text{ emu}$), when the magnet is operated in its persistent mode.

The temperature of the sample is determined from the resistance of a resistance thermometer fixed to the wall of the cryostat close to the sample. The resistance thermometer was an epoxy-resin potted slice taken from a 220- Ω Allen-Bradley resistor. It was calibrated in situ against a factory-calibrated germanium thermometer. Below 100 K the precision of the temperature determination is better than 1%. Above 100 K the sensitivity of the resistance thermometer is insufficient; the sample temperature is therefore determined from the voltage of a Au(0.03% Fe)-chromel thermocouple linked to the temperature-regulated diffusor. The variation of flow-dependent thermal gradients which can amount to several degrees will cause a considerable uncertainty in sample temperature for this range of temperatures.

Theory

Spin Hamiltonian. We will consider the interaction of six spins, localized at the cornerpoints of a regular octahedron. The spins are assumed to be coupled by an isotropic Heisenberg exchange interaction. This *intracluster* interaction can be described with the spin Hamiltonian

$$\hat{H} = -\frac{1}{\hbar^2} \sum_{i \neq j} J_{ij} \hat{S}^i \cdot \hat{S}^j \quad (1)$$

We will restrict the discussion to nearest-neighbor interactions only; $J_{ij} = J$ for nearest neighbors; $J_{ij} = 0$ for all other pairs. For this approximation the Hamiltonian will reduce to eq 2.

$$\hat{H} = -\frac{2J}{\hbar^2} \sum_{\substack{i < j \\ \text{nearest} \\ \text{neighbors}}} \hat{S}^i \cdot \hat{S}^j = -\frac{2J}{\hbar^2} \sum_{\substack{i < j \\ \text{nearest} \\ \text{neighbors}}} \left\{ \hat{S}_z^i \hat{S}_z^j + \frac{1}{2} (\hat{S}_+^i \hat{S}_-^j + \hat{S}_-^i \hat{S}_+^j) \right\} \quad (2)$$

Symmetry of the Hamiltonian. As a first step we will explore the symmetry properties of the Hamiltonian. For the total spin momentum operator $\hat{S} = \sum \hat{S}^i$ which is the sum of single-electron spin momentum operators \hat{S}^i we can verify that $[\hat{S}_z, \hat{H}] = [\hat{S}^2, \hat{H}] = 0$. Therefore both the total spin, S , and the z component of the total spin, $m_s = \sum m_s^i$, are good quantum numbers to describe the eigenstates of this Hamiltonian. The geometrical (in our case octahedral) symmetry is contained in the numbering over nearest neighbors: the Hamiltonian is invariant for the transformations which leave the octahedron invariant. Some of the symmetry transformations and the numbering of the Cu(II) sites are shown in Figure 2. The octahedron has a center of symmetry; the symmetry group is $O_h = O \times i$.

The eigenstates of the Hamiltonian will reflect the octahedral symmetry and can be labeled according to irreducible

(7) van Kempen, H.; Perenboom, J. A. A. J.; Wyder, P., to be submitted for publication.

(8) Gelsing, R. R.; van Kempen, H. "Proceeding of the 4th International Cryogenic Engineering Conference"; IPC Science and Technology Press, Ltd.: Surrey, 1972; p 233.

(9) Poerschke, R.; Wollenberger, H. *Cryogenics* 1976, 10, 333.

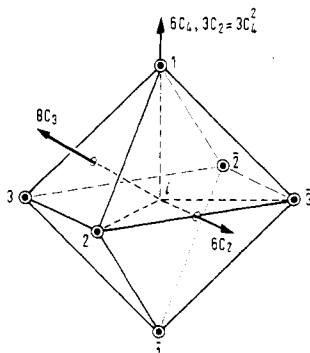


Figure 2. Symmetry operations of the octahedron. *i* is a center of inversion. An element is shown from each of the different classes of symmetry operations of the group O_h . The numbering of the Cu(II) sites is shown.

representations of the symmetry group of the octahedron.

Solving for the Eigenvalues. As a basis we take the 2^6 possible products of six single-electron spin functions (e.g., $\alpha(1)\alpha(\bar{1})\alpha(2)\alpha(\bar{2})\alpha(3)\alpha(\bar{3})$ for $m_s = 3$ and $\beta(1)\alpha(\bar{1})\alpha(2)\alpha(\bar{2})\alpha(3)\alpha(\bar{3})$ and the five different permutations for $m_s = 2$, etc.). On this basis we can evaluate the Hamiltonian in a simple way. For each of these basis functions we know $m_s = \sum m_s^i$. Only matrix elements between states with the same value of m_s can be nonzero.

The coupling of the six spins is dictated by the symmetry of the rotation group. The 2^6 states which are products of single-electron spin functions can be combined to functions which transform as irreducible representations of the rotation group; i.e., they have a well-defined spin quantum number S . The problem is well-known for two spins: the 2^2 product functions separate into a singlet $D^{(0)}$ and a triplet $D^{(1)}$, where $D^{(L)}$ is an irreducible representation of the rotation group with momentum quantum number L . Similarly for six spins

$$D^{(1/2)} \otimes D^{(1/2)} \otimes D^{(1/2)} \otimes D^{(1/2)} \otimes D^{(1/2)} \otimes D^{(1/2)} = D^{(3)} \oplus 5D^{(2)} \oplus 9D^{(1)} \oplus 5D^{(0)} \quad (3)$$

A similar result can be obtained with a less transparent formula given by van Vleck (see ref 10). There will be only one eigenstate of the Hamiltonian, which is simultaneously an eigenfunction of the operator \hat{S}^2 with an eigenvalue $S = 3$; this level is $(2S + 1)$ -fold degenerate when the m_s degeneracy is not lifted. There are five different quintuplets with $S = 2$, nine triplets with $S = 1$, and finally five singlets with $S = 0$ (altogether $64 = 2^6$ states).

When all pair interactions are equal, the Hamiltonian of eq 1 can be evaluated analytically by a generalized method.¹⁰ This method is exact only for a dimer, an equilateral triangular trimer, and a tetrahedron, where all pair interactions are indeed equivalent. When this model is applied to the more complex problem of the Hamiltonian of eq 2, where not all pair interactions are equivalent, the solution is not exact. In that case this model reduces to a mean field approximation. The remaining pair interactions are added, and the exchange constant J is rescaled accordingly.

We have solved the matrix given by the Hamiltonian of eq 2 numerically. The matrix elements were evaluated on the

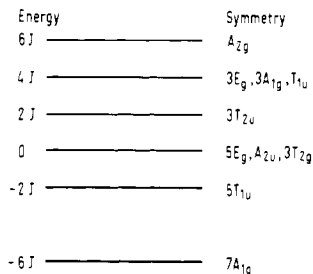


Figure 3. Energy level scheme calculated from the Hamiltonian defined in eq 2. The eigenstates are labeled according to the irreducible representations of the symmetry group O_h of the octahedron; the $(2S + 1)$ -fold degeneracy of the states indicates the total spin quantum number S .

basis of product functions. The spin quantum number of the eigenstates belonging to a particular eigenvalue was deduced from the occurrence of this eigenvalue in multiplets with different eigenvalue m_s . The eigenvalue equations were solved, and the symmetry of the eigenstates was determined from the transformation properties of the eigenstates under the symmetry transformations of the octahedral group. The symmetry of the levels can alternatively be deduced by a pure group theoretical a priori approach. The transformation properties under O_h of the basis functions which span a subspace with a particular value of m_s (e.g., the six functions for $m_s = 2$ mentioned earlier) can easily be determined by inspection. The characters of the representation so obtained allow a decomposition into the relevant irreducible representations in the usual way. The eigenstates have been labeled according to irreducible representations of O_h . In Figure 3 a summary is presented of the results of these calculations. The eigenstates have been determined and are listed as supplementary material.

Calculation of the Magnetic Susceptibility. We can calculate the magnetization induced by an external field when we include the Zeeman term in the Hamiltonian (eq 4). This

$$\hat{H} = -\frac{2J}{\hbar^2} \left[\sum_{\substack{i < j \\ \text{nearest} \\ \text{neighbors}}} \left\{ \hat{S}_z^i \hat{S}_z^j + \frac{1}{2} (\hat{S}_+^i \hat{S}_-^j + \hat{S}_-^i \hat{S}_+^j) \right\} \right] - \frac{\mu_0 g \mu_B H}{\hbar} \hat{S}_z \quad (4)$$

Hamiltonian reduces to the Hamiltonian of eq 2 for $H = 0$. As the eigenstates of the Hamiltonian in eq 2 are simultaneously eigenstates of the operator \hat{S}_z , the Zeeman term will contribute diagonal elements only; it leads to a $(2S + 1)$ -fold splitting of the energy levels proportional to m_s . The magnetization $M(H, T)$ can be calculated when the structure of the energy spectrum is known. The energy spectrum, for given exchange interaction constant J , can be derived from Figure 3 when the appropriate Zeeman terms are applied. Using the expression for the free energy F in terms of the partition function Z (eq 5), we can find the magnetization from

$$F(H, T) = -k_B T \ln Z = -k_B T \ln \left[\sum_n e^{-E_n(H)/k_B T} \right] \quad (5)$$

eq 6. When, moreover, the applied magnetic field is small,

$$M(H, T) = \frac{1}{\mu_0} \frac{\partial}{\partial H} F(H, T) \quad (6)$$

the magnetic susceptibility is found as the derivative of $M(H, T)$ with respect to H . In the present investigation the magnetization is not linearly dependent on H in magnetic fields on the order of 1 T and at the lowest temperatures. Therefore we have used the full magnetic field dependence contained in eq 5 and 6 for the comparison of the theory with the experimental data.

(10) Boudreaux, E. A.; Mulay, L. N. "Theory and Applications of Molecular Paramagnetism"; Wiley: New York, 1976; Chapter 7.

(11) For the copper-MIBA cluster we have used a diamagnetic correction of $-1.65 \times 10^{-8} \text{ m}^3/\text{mol}$; the atomic contributions were taken from the appendix of ref 10. The conversion from cgs to MKSA values is as follows: for the volume susceptibility $\chi^{\text{MKS A}} = 4\pi \chi^{\text{cgs}}$ and it is dimensionless; for the mass susceptibility $\chi^{\text{MKS A}} = (4\pi \times 10^{-3}) \chi^{\text{cgs}}$ and the dimension is m^3/kg ; for the molar susceptibility $\chi_M^{\text{MKS A}} = (4\pi \times 10^{-6}) \chi_M^{\text{cgs}}$ and the dimension is m^3/mol ; for the magnetic moment $1 \text{ J/T} = 10^3 \text{ emu}$.

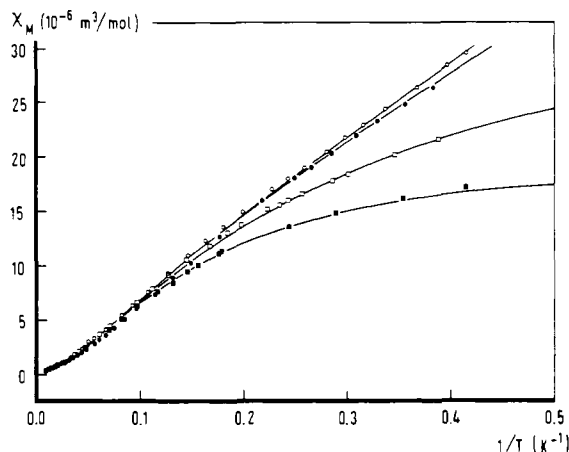


Figure 4. Static magnetic susceptibility of the copper-MIBA cluster measured at different values of the applied magnetic field (○, 0.185 T; ●, 0.400 T; □, 1.20 T; ■, 2.00 T). The solid lines correspond to the theory described in the text. The following parameters have been used: exchange constant $J/k_B = 7.3$ K; number of clusters = 0.334 mol/kg; temperature-independent background $\chi_M(T \rightarrow \infty) = -6.3 \times 10^{-8}$ m³/mol; also a weak antiferromagnetic interaction was taken into account with $\Theta = -0.14$ K to get a better fit to the low-temperature data (see text).

Discussion of the Results

We have compared the magnetization data with the temperature and field dependence predicted by the theory presented in the previous section. The magnetic moment of the samples was measured at different values of the applied magnetic field. The static susceptibility was calculated from these data by using the equation $m = (w/m_M)\chi_M H$. Here m is the magnetic moment in units of J/T, w is the mass of the sample in kg, m_M is the mass of 1 mol in kg, χ_M is the molar susceptibility in MKSA units (m³/mol),¹¹ and H is the strength of the applied magnetic field in A/m. The data for the copper cluster with H₂MIBA ligands are presented in Figure 4. The plot shows a close agreement between theory and experiment.

We have adjusted four parameters to compare the experimental data with the theory.

(i) First of all the vertical scale is determined by the Curie constant which is proportional to the number of paramagnetic moments and proportional to the square of the effective Bohr magneton number [$\mu_{\text{eff}}^2 = g^2 S(S+1)$]. The number of spins was deduced from the chemical analysis. Possible variations of the amount of water of crystallization leads to an uncertainty in this factor of several percent. In our calculations we have taken the free-electron value for the g factor.

(ii) Second, a temperature-independent contribution to the magnetization is inherent to the measurement technique. This contribution is due to the diamagnetic susceptibility of the sample material itself and to the diamagnetic susceptibility of sample cup and support rod; as this latter contribution is strongly dependent on their exact positions relative to the pickup coils, it is not possible to determine a very accurate background correction. We have determined the diamagnetic background $\chi_M(T \rightarrow \infty)$ from a simultaneous fit of the Curie law to the data at the highest temperatures for all the different values of applied magnetic field; as we will discuss later, the Curie constant ($C = \chi_M T$) so obtained is higher than deduced from the chemical analysis.

(iii) The third parameter is the strength of the exchange interaction J/k_B . This is the only free parameter which enters the theory.

(iv) We have also explored the influence of an additional weak interaction, due to for instance *intercluster* interactions. The low-temperature data are systematically lower than the value predicted by the theory for any reasonable choice of J ,

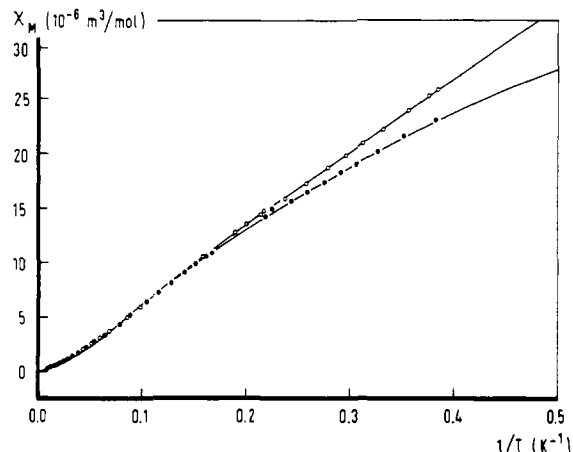


Figure 5. Static magnetic susceptibility of the copper-Pen cluster measured at different values of the applied magnetic field (○, 0.20 T; ●, 0.80 T). The solid lines correspond to the theory described in the text. The following parameters have been used: exchange constant $J/k_B = 6.9$ K; number of clusters = 0.220 mol/kg; temperature-independent background $\chi_M(T \rightarrow \infty) = -7.4 \times 10^{-8}$ m³/mol.

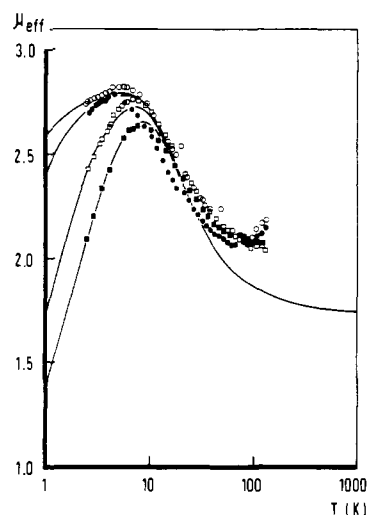


Figure 6. Plot of the effective Bohr magneton number for the copper-MIBA complex. The solid line is calculated from the theory described in the text with the same parameters as used in Figure 4.

both for the copper-MIBA cluster and for the copper-Pen cluster. The fit can be improved by a lowering of the Curie constant by a few percent. For the copper-MIBA cluster, however, a much better fit could be found with an additional antiferromagnetic interaction, introduced as factor $T/(T - \Theta)$ for a value $\Theta = -0.14$ K. This resulted in a better agreement in both the detailed temperature dependence and the magnitude of the susceptibility at low temperature.

It is clear from Figure 4 that with the choice of the parameters discussed above a very good description can be given of the field and temperature dependence of the magnetic susceptibility for the copper-MIBA complex. The data for the copper-Pen complex would require an antiferromagnetic interaction of -0.35 K to match the magnitude of the low-temperature data, but the detailed temperature dependence at low temperatures can be better described with $\Theta = 0$ K and with a reduced Curie constant (90%). The agreement between the theory and experimental data, for $\Theta = 0$ K and for a reduced Curie constant, is shown in Figure 5 for the copper-Pen cluster. The reduction of the Curie constant may be due to a reduction of the effective g value, as will be discussed below. The value of Θ reported for the copper-DMC complex is much higher (-2.5 to -3.0 K).⁵ The value of this Θ found

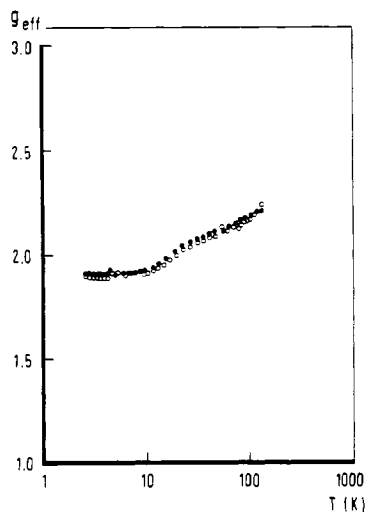


Figure 7. Variation of the effective g factor required to bring the theory described in the text in accordance with the experimental data for the copper–Pen cluster. At low temperatures g_{eff} is slightly less than the free-electron value. The symbols refer to the different values of the applied magnetic field (O, 0.20 T; ●, 0.80 T).

from a least-square fit of our model to the published data of this complex is substantially reduced because the field dependence is properly accounted for. As with copper–Pen, a value $\theta = 0$ would be in better agreement with the temperature dependence of the susceptibility data.

Also at the high-temperature side there remains some mismatch between the data and the theoretical model, as is shown in Figure 6. Both for the copper–MIBA and for the copper–Pen cluster the Curie–Weiss law which gives a best fit to the data in the high-temperature region ($T > 80$ K) has a Curie constant which is significantly larger than calculated from the chemical composition of the samples. We have measured the susceptibility of the copper–MIBA cluster with Gouy's method in the temperature range from 100 to 250 K. The effective bohr magneton number was calculated from these data after correction for the diamagnetic contribution of the constituents,¹¹ and it was found that $\mu_{\text{eff}} = 2.06 \pm 0.06$. This value is compatible within 1% with the Curie constant found from a least-squares fit to the magnetization data of the form $m(T) = \chi_M(T \rightarrow \infty)H + CH/T$. The increase over the expected high-temperature limiting value $(g^2S(S+1))^{1/2}$

$= 1.73$ can be due to partial ordering in this temperature range, but the data at lower temperatures do not allow the necessary increase of the ferromagnetic interaction J within the present model. Because of the deviation from the theory at high and low temperatures, it is not possible to determine the exchange interaction constant very reliably; we have found $J/k_B = 7 \pm 1$ K for the copper–MIBA complex and a somewhat weaker exchange interaction $J/k_B = 6 \pm 1$ K for the copper–Pen complex.

Because the additional antiferromagnetic interaction did not improve the fits for the copper–Pen cluster, we have set this parameter to zero again, and only three parameters are left to describe the magnetization. As discussed above, the scale factor is fixed by the chemical analysis; the asymptotic value $\chi_M(T \rightarrow \infty)$ can be found by extrapolation of the Curie law with a Curie constant which is higher than expected. Adjustment of merely the exchange constant J , the only free parameter left, does not lead to an accurate description of the magnetization data.

The mismatch between the present theory and the experimental data can be attributed tentatively to a variation of the effective g factor. In Figure 7 it is shown, how the g factor should vary for the copper–Pen cluster to obtain a match between the present theory and the data. A similar variation has been found for the copper–MIBA complex. The high value of the effective g value found at high temperatures may be an indication that partial ordering of the spins is already effective in this temperature region. We are currently investigating whether deviations from the octahedral symmetry can account for this phenomenon.

Acknowledgment. The assistance of Mr. J. J. Bour for the measurements of the susceptibility with the Gouy method is gratefully acknowledged. Part of this work has been supported by the Stichting voor Fundamenteel Onderzoek der Materie (FOM) with financial support from the Nederlandse Organisatie voor Zuiver Wetenschappelijk Onderzoek (ZWO).

Registry No. $[\text{Co}(\text{NH}_3)_6]_5[\text{Cu}_{14}(\text{Pen})_{12}\text{Cl}]_3$, 64916-24-1; $[\text{Co}(\text{NH}_3)_6]_5[\text{Cu}_{14}(\text{MIBA})_{12}\text{Cl}]_3$, 71786-24-8; $\text{Na}_5[\text{Cu}_{14}(\text{Pen})_{12}\text{Cl}] \cdot x\text{H}_2\text{O}$, 65028-63-9; $\text{Na}_5[\text{Cu}_{14}(\text{MIBA})_{12}\text{Cl}] \cdot x\text{H}_2\text{O}$, 76036-34-5; $\text{Co}(\text{NH}_3)_6\text{Cl}_3$, 14695-95-5.

Supplementary Material Available: Listings of the measured and calculated values of the magnetic moment and of the eigenstates of the Hamiltonian (9 pages). Ordering information is given on any current masthead page.